Machine Learning Optimization of BEGe Detector Event Selection in the VIP Experiment

S. Manti[1,*,†] **S.H. Yip**[2,†] **M. Bazzi**[1] **N. Bortolotti**[1,3] **M. Bragadireanu**[4] **M. Cargnelli**[5,6] **I. Carnevali**[1] **A. Clozza**[1] **L. De Paolis**[1] **R. Del Grande**[7,1] **C. Guaraldo**[1,‡] **M. Iliescu**[1] **M. Laubenstein**[8] **J. Marton**[5,6] **F. Napolitano**[9,10] **F. Nola**[1] **K. Pischicchia**[1,3] **A. Porcelli**[11,12] **A. Scordo**[1] **F. Sgaramella**[1] **D. Sirghi**[3,1,4] **F. Sirghi**[1,4] **J. Zmeskal**[5,‡] **C. Curceanu**[1,4]

[1] *Laboratori Nazionali di Frascati INFN, Frascati, Italy*

[2] *University of California, Berkeley, CA 94720, USA*

[3] *Centro Ricerche Enrico Fermi, Museo Storico della Fisica e Centro Studi e Ricerche "Enrico Fermi", Roma, Italy*

[4] *IFIN-HH, Institutul National pentru Fizica si Inginerie Nucleara Horia Hulubei, 30 Reactorului, 077125, Magurele, Romania*

[5] *Stefan Meyer Institute for Subatomic Physics, Vienna, Austria*

[6] *Atominstitut, Technische Universität Wien, Stadionallee 2, 1020 Vienna, Austria*

[7] *Faculty of Nuclear Sciences and Physical Engineering, Czech Technical University in Prague, Břehovà 7, 115 19, Prague, Czech Republic*

[8] *Laboratori Nazionali del Gran Sasso, Istituto Nazionale di Fisica Nucleare, Via G. Acitelli 22, 67100, Assergi, Italy*

[9] *Via A. Pascoli 06123, Perugia (PG), Italy, Dipartimento di Fisica e Geologia, Università degli studi di Perugia*

[10] *INFN Sezione di Perugia, Via A. Pascoli, 06123 Perugia, Italia*

[11] *Centro de Investigacíon, Tecnología, Educacíon y Vinculacíon Astronómica, Universidad de Antofagasta, Avenida Angamos 601, 1240000, Antofagasta, Chile*

[12] *Faculty of Physics, Astronomy, and Applied Computer Science, Jagiellonian University, Kraków, Poland*

* *Corresponding Authors*

† *These authors contributed equally*

‡ *Deceased*

E-mail: simone.manti@lnf.infn.it, jason17@berkeley.edu

Abstract: Experiments that probe the foundations of quantum mechanics require detectors with excellent sensitivity at low energies and very low background rates. In this context, the VIP collaboration operates a Broad-Energy Germanium (BEGe) detector at the Gran Sasso National Laboratory to monitor background radiation in the few-keV to 100 keV range. We present a machine-learning–based upgrade to the data acquisition and event-selection strategy aimed at improving the detection of low-energy events up to 10 keV. The method employs a denoising autoencoder to suppress electronic and microphonic noise and reconstruct pulse shapes, followed by a convolutional neural network that classifies waveforms as normal single-site or anomalous events. The workflow was validated on a dataset which consits of more than 20000 waveforms recorded in 2021. The classifier achieves an area under the ROC curve of 0.99 and an accuracy of 95% and applying this procedure lowers the effective energy threshold to approximately 10 keV. It also yields a measurable enhancement in spectral quality, including an improvement of about 20% in the signal-to-background ratio and an energy resolution of about 1 keV at 100 keV for the characteristic Pb and Bi gamma lines. These developments enhance the sensitivity of the BEGe detector to rare low-energy signals and provide a scalable framework for future precision tests of quantum foundations in low-background environments.

Keywords: VIP, BEGe, Machine Learning

Contents

1 Introduction

Experimental tests of the foundations of quantum mechanics require extreme sensitivity, as they target phenomena that, if observed, would occur at very reduced rates. Such rare-event searches provide a unique window into possible deviations from the standard quantum framework, complementing more conventional precision tests and opening opportunities to probe new physics at the interface between microscopic and macroscopic scales [1, 2]. Among the most fundamental principles of quantum theory is the Pauli Exclusion Principle (PEP) [3], which underlies the structure of atoms, the stability of matter [4], and even the behavior of astrophysical objects like neutron stars [5]. Its validity is directly linked to the Spin–Statistics Theorem [6], which dictates that fermions (bosons) obey antisymmetric (symmetric) wave functions under exchange of particles. Any violation of PEP would have profound implications, pointing to physics beyond the established quantum framework. From an experimental point of view, such violations could manifest as examples of anomalous atomic transitions, shifted by a few tenths of a keV from the standard spectral lines [7]. Establishing increasingly stringent limits on such effects is therefore a central goal of dedicated rare-event searches. Another direction involves models of spontaneous wave-function collapse, which attempt to resolve the measurement problem by introducing additional physical mechanisms that suppress quantum superpositions at macroscopic scales. Prominent examples include the Continuous Spontaneous Localization (CSL) model [8] and the Diósi–Penrose (DP) model [9, 10]. Both predict the spontaneous emission of radiation, in particular X-rays in the keV range, which can serve as experimental signatures of the particular collapse model especially in the low-energy regime [11]. Detecting such rare and subtle signatures requires not only excellent energy resolution but also extremely low background. Underground laboratories play a crucial role in this context. The Gran Sasso National Laboratory (LNGS) provides a uniquely low-background environment for the study of rare events. Located under approximately 1400 m of rock-equivalent to 3800 m w e water-equivalent (m w.e.), the overburden reduces the cosmic muon flux to only about $3.41 \times 10^{-4} \, \mathrm{m}^{-2} \, \mathrm{s}^{-1}$ [12]. This substantial attenuation of the muon flux enables experiments at LNGS to achieve significantly reduced background levels. This makes LNGS one of the world's premier environments for rare-event searches, hosting experiments ranging from neutrino physics to dark matter and double beta decay [13–15]. Within this environment, the VIP (Violation of the Pauli Exclusion Principle) collaboration has progressively tightened the upper limits on PEP-violating events. The original VIP experiment set an upper limit of $\beta^2/2 < 4.7 \times 10^{-29}$ [16], the most stringent constraint at the time. Its successor, VIP-2, pushed this further, establishing limits of $\beta^2/2 \leq 6.8 \times 10^{-42}$ (Bayesian, 90% CL) and $\beta^2/2 \leq 7.1 \times 10^{-42}$ (Frequentist CL_s, 90% CL) [17]. The ongoing VIP-3 effort is extending the search across the periodic table, with high-Z targets such as zirconium, silver, palladium, and tin [18]. A central element of these experiments is the detector technology. Broad Energy Germanium (BEGe) detectors combine the features of coaxial and low-energy HPGe designs, covering a wide dynamic range from a few keV up to several MeV. They are particularly suited for rare-event
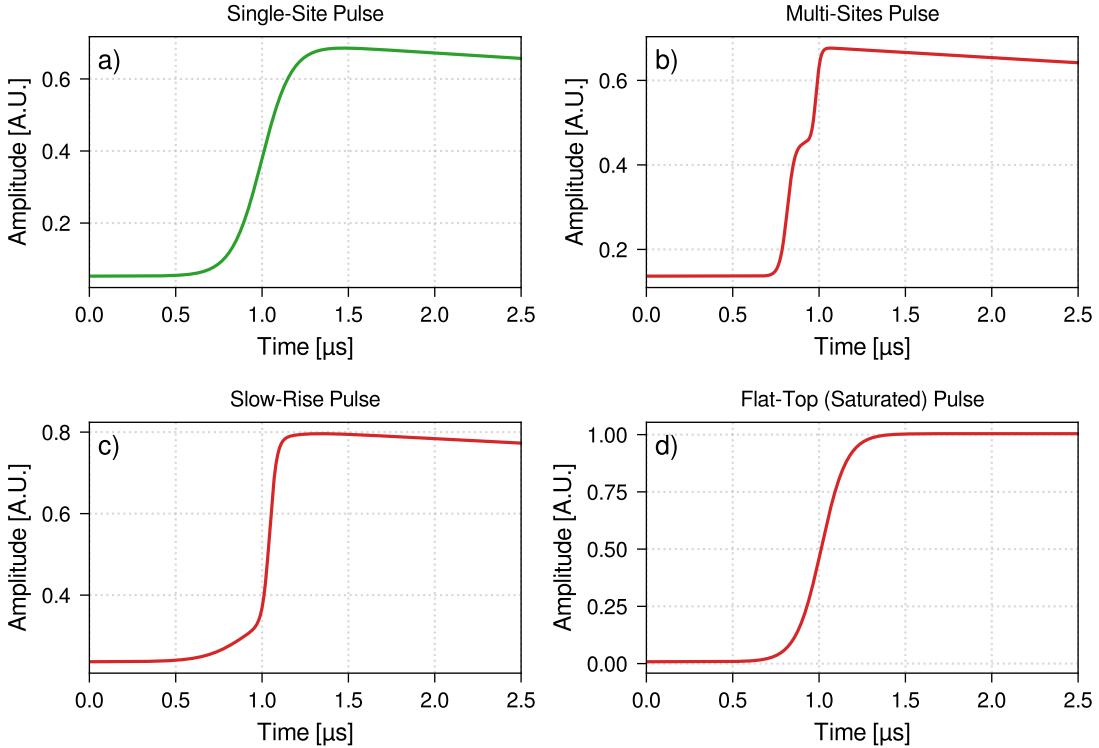
searches because of their excellent resolution and efficiency at low energies. However, achieving thresholds of a few keV is challenging due to microphonic noise and electronic instabilities, which can obscure faint signals precisely in the energy range of interest for PEP-violating transitions and collapse-induced radiation [11]. In recent years, machine-learning techniques have emerged as powerful tools for improving pulse-shape analysis and low-energy event selection in germanium detectors, enabling discrimination between single-site and multi-site interactions and identification of event classes relevant for rare-event searches such as neutrinoless double-beta decay. In this work, we report recent advances in the operation of a BEGe detector within the VIP program at LNGS. Two key improvements were implemented. First, the detector setup was mechanically and acoustically isolated using a soundproof box and pneumatic suspension, suppressing microphonic contributions. Second, we developed and validated a machine–learning–based event selection strategy, employing a denoising autoencoder and a convolutional neural network to enhance discrimination between signal and background. These methods were applied to data acquired in 2021, demonstrating improved effective energy threshold and a higher signal-to-background ratio. The remainder of this paper is organized as follows. Section 2 describes the experimental setup, including the BEGe detector and its isolation system. Section 3 introduces the machine-learning framework for event selection, with emphasis on the denoising and classification stages. Section 4 presents the performance validation with the 2021 dataset and discusses the improvements in resolution, threshold, and background rejection. Section 5 concludes with a summary and an outlook for future developments in the VIP program and related rare-event searches.

2   BEGe Event Selection Strategy

Event selection was performed using pulse shape analysis (PSA) on the acquired waveforms of the BEGe setup. To automate this selection and integrate it in the data acquisition, we employed deep learning with a Denoising Autoencoder (DAE) [19] with two main objectives. First, to remove noise from the waveforms and improve the selection of low-energy events. Second, to extract features that help in distinguishing normal events from anomalous ones (e.g. multi-site, saturated, and similar events). The latter is important for the creation of a dataset for supervised training of a classifier connected to the output of the DAE, allowing for anomaly detection of events.

This ML-aided PSA procedure was validated using the data collected in 2021 [11], which consist of more than 20000 events. For each event, a waveform is recorded by the BEGe detector electronics through a 400 MHz digitizer spanning 1024 samples, giving a total acquisition window of 2.55 μs. Further details on the BEGe apparatus are provided in our previous article [11]. We implemented the DAE within the Keras framework (v3.5.0). The DAE, which in input is operating on both the waveform and its derivative, is based on a one-dimensional (1D) convolutional neural network (CNN) with an encoding and decoding structure. The encoder comprises three convolutional layers with progressively decreasing filter sizes (i.e. 64, 32, 16), each followed by the rectified linear unit (ReLU) activation function, and max-pooling operations. The temporal dimension of the waveform in the input layer was reduced to 128 to decrease network complexity and shorten training time. The chosen input size and number of hidden layers represent a balance between model complexity, training efficiency, and the performance of both the DAE and the attached classifier. The decoder mirrors the encoder structure, using upsampling layers and additional convolutional layers with ReLU activation to restore the original waveform, followed by a final convolutional layer with linear activation to produce the reconstructed signal. The model is trained using the Adam optimizer with a learning rate of 10^{-4}. No hyperparameter tuning was required, since both the DAE and the CNN classifier achieved excellent performance with their initial configurations.

To train the DAE, we created a synthetic dataset of pulses that resemble the typical scenarios of events in our BEGe detector setup (see Figure 1). A normal event (see Figure 1a) corresponds to single-site energy depositions occurring within the bulk of the germanium detector, where the electric field is uniform and charge carriers are efficiently collected at the electrodes. These events are characterized by a prompt, steep rising edge and an exponential decay, and represent the expected signal. Multi-site pulses (see Figure 1b) are

Figure 1. Examples of the four pulse types in the synthetic dataset used to train the Denoising Autoencoder: a normal pulse (green) in panel a, and anomalous pulses (red): multi-site (panel b), slow-rise (panel c), and saturated (panel d).

generated to mimic the response to events in which energy is deposited at multiple, spatially separated locations within the detector volume. Such events can arise from, for example, Compton scattering or coincident background interactions. The resulting pulse shapes typically exhibit multiple rising steps or a more complex rise profile, reflecting the superposition of charge collection from each interaction site. Slow-rise pulses (see Figure 1c) are included to model interactions occurring near the detector surfaces, where the electric field strength is reduced. In these regions, charge carriers drift more slowly to the electrodes, resulting in a notably slower rise time compared to bulk events. The inclusion of slow-rise pulses in the training set allows the DAE to learn features associated with surface backgrounds, which can be subsequently suppressed through pulse shape discrimination, thereby improving the overall signal-to-noise ratio. Flat-top (see Figure 1d) are also incorporated in the dataset. These pulses are characterized by a rapid rise followed by a plateau, which can occur when the detector response saturates due to high-energy depositions or limitations in the readout electronics. Including flat-top pulses in the training set is crucial to ensure that the DAE can recognize and appropriately process saturated signals, which may otherwise be misidentified or improperly reconstructed. These categories follow the standard classification established in BEGe pulse shape analysis studies [20–22]. Each simulated pulse was superimposed with noise to reproduce the conditions of the experimental setup. Two noise components were considered: (i) white Gaussian noise, representing intrinsic electronic fluctuations, and (ii) colored noise generated by integrating a white noise process to emulate the low-frequency microphonic and environmental instabilities observed in the detector. The relative amplitude of the two components was tuned to match the baseline noise spectrum previously characterized for the BEGe setup [11]. Two distinct noise levels were applied, yielding a total of 5000 simulated events evenly divided between high- and low-noise conditions. This approach ensured that the DAE was trained across realistic noise

environments, thereby improving its robustness when applied to experimental data.
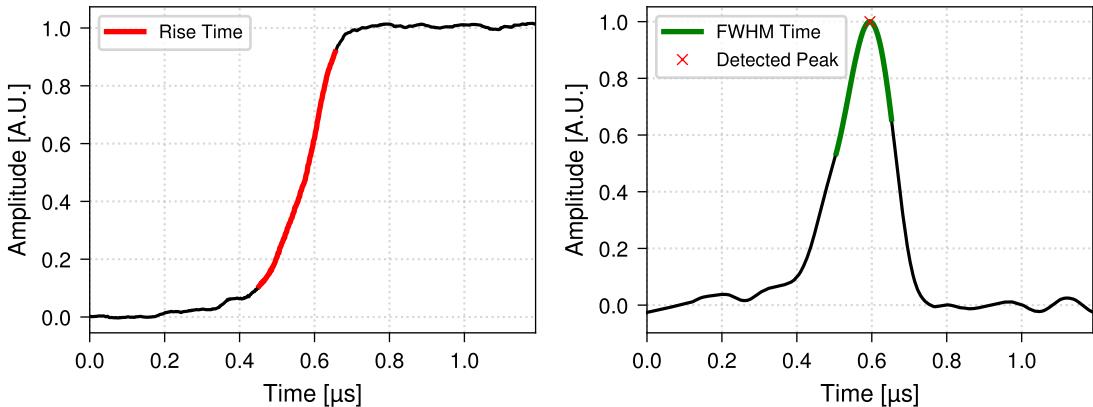
All events are preprocessed prior to training through baseline subtraction and normalization by their amplitude. For each pulse, the baseline is first estimated as the mean of the initial 100 samples and subtracted from the entire waveform to remove DC offsets. The resulting signal is then processed with a trapezoidal filter [23], and the amplitude is extracted as the maximum absolute value of the filtered output beyond the filter response region. The baseline-subtracted pulse is then normalized by this amplitude, resulting in a unit-amplitude, baseline-corrected signal. This standardized preprocessing pipeline is applied uniformly to both synthetic and experimental datasets to ensure robust and consistent inputs throughout model training and evaluation. It is worth noting that without this baseline subtraction and normalization, the DAE fails to accurately reconstruct pulse shapes.

The reconstructed pulses produced by the DAE serve as inputs for the binary CNN classifier for anomaly detection of events. Each event has two input channels: the normalized pulse taken from the DAE output, which needs no further normalization, and the normalized first derivative of the pulse scaled to the range $[0, 1]$. Using both the pulse and its first derivative as separate channels allows the CNN to learn the relation between the pulse shape and small changes such as multi site events.

To then train the classifier we create a dataset of waveforms with labels. We do this by selecting features from the output of the DAE and placing constraints on their distributions. As features we use:
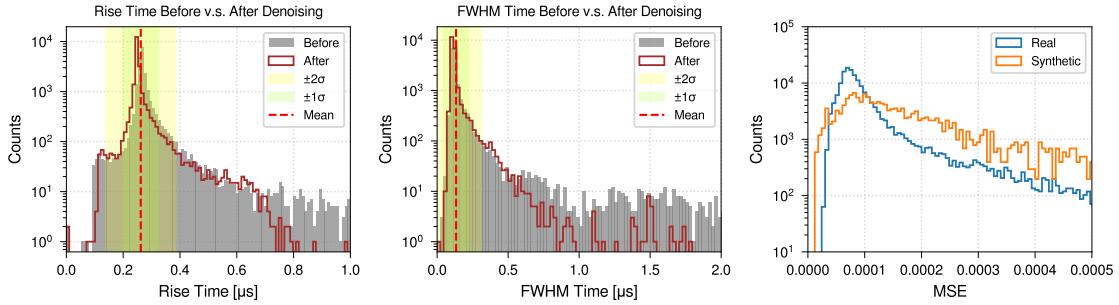
- Rise time: the time needed for the waveform to rise from 10% to 90% of its amplitude.

- Number of peaks in the first derivative of the waveform.

- FWHM time: the duration of the full width at half maximum of the derivative for events with only one peak in the derivative.

- The L1 norm of the waveform with respect to the average pulse.

A visual inspection of the rise time and FWHM time is shown in figure (2).

Figure 2. The rise time (left) is defined as the interval between 10% and 90% of the waveform amplitude (red). The FWHM time (right) is defined from the derivative of the waveform, with the FWHM interval highlighted in green.
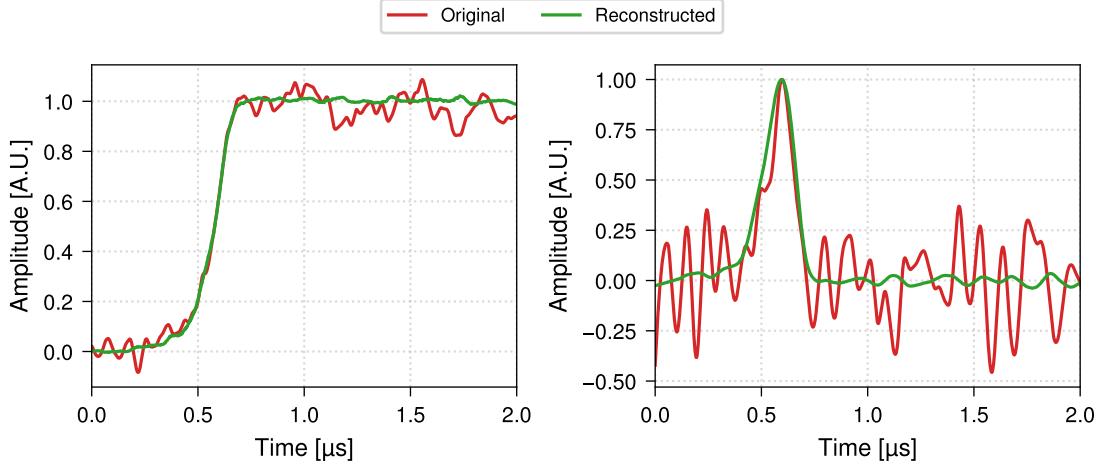
To check that extracting features from the output of the DAE is a valid approach, we calculate the rise time and FWHM time for all data before and after cleaning the waveforms with the DAE, as shown in figure (3). The DAE does not change the features within $\pm\sigma$ of the main peak. This shows that the cleaning procedure does not distort the waveforms and supports the validation of the DAE from synthetic data to real data. To support this further we also show in figure 4 the mean squared error (MSE) of the DAE on real and

Figure 3. Rise time (left) and FWHM time (center) distributions for the events before and after applying the DAE, with mean and variance intervals. On the right is the mean squared error (MSE) of the DAE on the real and synthetic waveform data.

synthetic data. The DAE gives similar values on both datasets, which indicates that it generalizes well to real data. The larger tail in the synthetic data is due to the different noise level used in the construction of the synthetic dataset. The effect of the DAE on a low energy event, where the reduction of the background is clear, is shown in figure (4).

Normal events for training are defined as those that satisfy all of the following conditions:

Figure 4. Effect of the denoising autoencoder on a real waveform (left) and on its derivative (right) for a low-energy pulse which corresponds to an energy of ~15 keV.
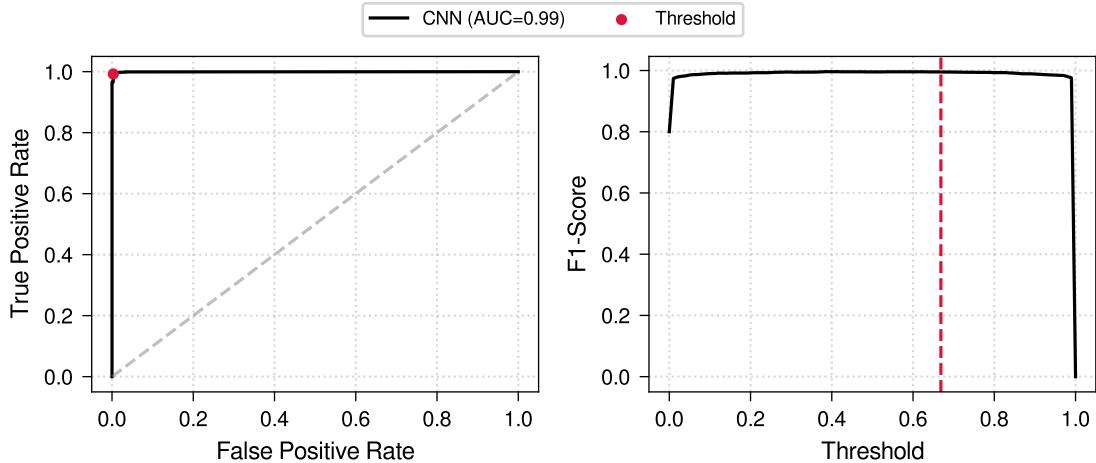
1. Feature constraints: the rise time, full width at half maximum (FWHM) time, and L1 norm each fall within one standard deviation (1σ) of their respective total distributions.

2. Peak count: the event contains exactly one peak in the normalized first derivative, as determined with the `find_peaks` function from SciPy.

3. Labeling: all waveforms are then manually labeled with a custom GUI program and assigned a signal label.

The resulting dataset is already well defined by the first two criteria, and manual labeling changes the selection by only 3%. To train the CNN classifier, the dataset was split in training, validation, and testing with proportions 70%, 15% and 15%, respectively. The CNN model is composed of sequential 1D convolutional layers

with increasing filter sizes (128,64,32) and decreasing kernel widths, each followed by batch normalization and max pooling to extract and condense features from the input. A fully connected dense layer interprets the extracted features, with a dropout layer included to mitigate overfitting. The final output layer uses a sigmoid activation function to produce a probability score for binary classification. The model is trained using the Adam optimizer with a learning rate of 10^{-5} and binary cross-entropy loss, and evaluated using accuracy, precision, and recall metrics. Early stopping of 10 epochs is employed to prevent overfitting and ensure optimal model weights.

3 Results and Discussion

The DAE–CNN workflow was applied to the 2021 BEGe dataset to evaluate its performance and improvements on the final spectrum and assess its suitability for integration into the online data-acquisition (DAQ) of the BEGe for VIP. After training, the CNN classifier assigns to each event the probability of being a normal (single-site) waveform. The classifier performance is quantified using the receiver operating characteristic (ROC) curve and the F1-score, as shown in Figure 5, resulting in an area under the curve (AUC) of 0.99. The optimal operating point is defined by the threshold that maximizes the F1-score, with an accuracy of 95 %. At this working point, approximately 13 % of events are rejected as anomalous. A feature-based classifier trained on rise time and FWHM also provides good separation power, but computing these features online would introduce significant computational overhead. In contrast, the CNN operates directly on the acquired waveform, maintaining high accuracy while remaining compatible with real-time inference, and allowing the DAQ system to store only classification results rather than full waveforms, thereby substantially reducing data volume. Events with classification probability above the optimal threshold are selected as
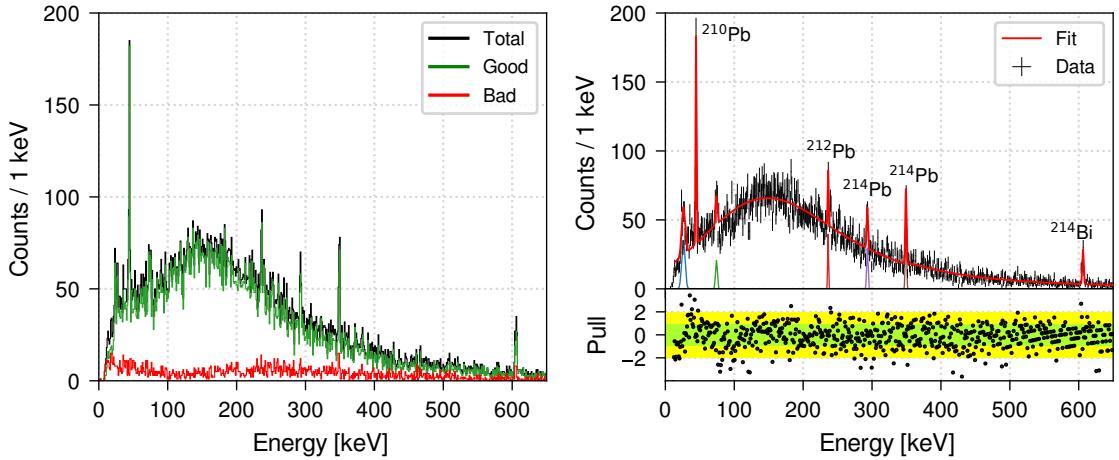

Figure 5. Performance of the CNN classifier applied to DAE-processed waveforms. Left: ROC curve with an AUC of 0.99, with the chosen operating threshold marked in red. Right: accuracy and F1-score as a function of the classification threshold, with the selected operating point indicated by the dashed red line.

normal (single-site) events. Spectra constructed by selecting events with the classifier can be divived as in Figure 6. To exctract the calibration a fit with binned maximum-likelihood approach was done. The calibration uses the four prominent gamma lines from the ^{238}U decay chain: ^{210}Pb at 46 keV, ^{214}Pb at 295 and 352 keV, and ^{214}Bi at 609 keV. Each spectrum is fitted with the following model:

$$f(x) = e^{a_1 + b_1 x} \frac{1}{2} \left[1 + \text{erf}\left(\frac{x - \mu_1}{\sigma_1}\right) \right] + e^{a_2 + b_2 x} \frac{1}{2} \left[1 + \text{erf}\left(\frac{x - \mu_2}{\sigma_2}\right) \right] + \sum_i A_i \exp\left(-\frac{(x - \mu_{g,i})^2}{2\sigma_{g,i}^2}\right).$$

The background is modeled using two error-function components, chosen to be just an empirical parameterization that provides a stable and reliable fit for the energy calibration. A physically motivated background model will be developed in future studies. The gamma lines are modeled with Gaussian functions. The fitted spectra and pull distributions are shown in Figure 6. Using the DAE–CNN event selection, the effective energy threshold is lowered to approximately 11 keV, and the energy resolution at the 46 keV line is measured to be in the range of 1.0–1.5 keV (FWHM). The DAE significantly suppresses noise-induced distortions in the sub-15 keV region, enabling reliable amplitude extraction at low energy. Without the DAE preprocessing,

Figure 6. Left: measured spectra after ML-based event selection, showing normal (green), anomalous (red), and total (black) events. Right: fitted spectrum (red) with individual Gaussian components (coloured) and pull distribution below.

the region below 15 keV is dominated by electronic noise and microphonic disturbances, limiting the depth of the analysis and reducing the sensitivity to low-energy processes. The DAE reconstructs physically plausible pulse shapes while suppressing noise components, significantly improving amplitude estimation and stabilizing the downstream classification. The ML-based selection enhances the signal-to-background ratio by approximately 14 %, with the largest improvement in the 10–50 keV region where anomalous waveforms contribute substantially to the background. Lowering the effective threshold to ~11 keV directly supports the physics goals of the VIP program by improving the sensitivity to rare low-energy processes. Moreover, the DAE preprocessing enables alternative analysis strategies beyond the CNN classifier, including traditional pulse-shape discrimination and feature-based ML methods based on rise time, FWHM, or waveform derivatives. A Python package, `vipbege`, is provided together with this work, offering tools to extract the waveform features discussed here and to generate simulated waveforms with or without noise. This makes the approach transferable to future BEGe datasets and adaptable to similar low-background detector configurations.

4   Conclusions

In this work we developed and validated a machine-learning–based event–selection strategy for a BEGe detector operated in the VIP experiment at LNGS. A denoising autoencoder, trained on synthetic waveforms representative of the main pulse classes, was used to suppress microphonic and electronic noise and to extract robust pulse-shape features. A CNN classifier attached to the DAE output enables fast event selection and anomaly detection. Applied to the 2021 dataset, the method achieves an AUC of 0.99 and 95% accuracy, lowers the effective energy threshold to about 10–11 keV, and improves the signal-to-background ratio by 20%. These results demonstrate that ML-based waveform cleaning can significantly enhance the low-energy

sensitivity of BEGe detectors, providing a valuable tool for future studies of collapse-model signatures and tests of the Pauli Exclusion Principle in low-background environments.

Data availability statement

The labeled dataset of 2021 BEGe waveforms used in this study is publicly available on Zenodo under the DOI: 10.5281/zenodo.17641589. All scripts required to reproduce the figures presented in this article are available at: `git@github.com:simonemanti/figures_bege.git`.

References

[1] S.L. Adler and A. Bassi, *Collapse models with non-white noises*, *Journal of Physics A: Mathematical and Theoretical* **40** (2007) 15083.

[2] A. Bassi, K. Lochan, S. Satin, T.P. Singh and H. Ulbricht, *Models of wave-function collapse, underlying theories, and experimental tests*, *Reviews of Modern Physics* **85** (2013) 471.

[3] W. Pauli, *The Connection Between Spin and Statistics*, *Physical Review* **58** (1940) 716.

[4] F.J. Dyson and A. Lenard, *Stability of Matter. I*, *Journal of Mathematical Physics* **8** (1967) 423.

[5] N.K. Glendenning, *Special and General Relativity: With Applications to White Dwarfs, Neutron Stars and Black Holes*, Springer Science & Business Media (Apr., 2010).

[6] R.F. Streater and A.S. Wightman, *PCT, Spin and Statistics, and All That*, Princeton University Press (2000).

[7] E. Ramberg and G.A. Snow, *Experimental limit on a small violation of the Pauli principle*, *Physics Letters B* **238** (1990) 438.

[8] G.C. Ghirardi, *Unified dynamics for microscopic and macroscopic systems*, *Physical Review D* **34** (1986) 470.

[9] L. Diósi, *Gravitation and quantum-mechanical localization of macro-objects*, *Physics Letters A* **105** (1984) 199.

[10] R. Penrose, *On Gravity's role in Quantum State Reduction*, *General Relativity and Gravitation* **28** (1996) 581.

[11] K. Piscicchia, A. Clozza, D.L. Sirghi, M. Bazzi, N. Bortolotti, M. Bragadireanu et al., *Optimization of a BEGe Detector Setup for Testing Quantum Foundations in the Underground LNGS Laboratory*, *Condensed Matter* **9** (2024) 22.

[12] G. Bellini, J. Benziger, D. Bick, G. Bonfini, D. Bravo, M.B. Avanzini et al., *Cosmic-muon flux and annual modulation in Borexino at 3800 m water-equivalent depth*, *Journal of Cosmology and Astroparticle Physics* **2012** (2012) 015.

[13] XENON Collaboration, E. Aprile, K. Abe, F. Agostini, S. Ahmed Maouloud, L. Althueser et al., *First Dark Matter Search with Nuclear Recoils from the XENONnT Experiment*, *Physical Review Letters* **131** (2023) 041003.

[14] Majorana Collaboration, C.E. Aalseth, N. Abgrall, E. Aguayo, S.I. Alvis, M. Amman et al., *Search for Neutrinoless Double-$\ensuremath{\beta}$ Decay in $^{76}\mathrm{Ge}$ with the Majorana Demonstrator*, *Physical Review Letters* **120** (2018) 132502.

[15] GERDA Collaboration, M. Agostini, G.R. Araujo, A.M. Bakalyarov, M. Balata, I. Barabanov et al., *Final Results of GERDA on the Search for Neutrinoless Double-$\ensuremath{\beta}$ Decay*, *Physical Review Letters* **125** (2020) 252502.

[16] S. Bartalucci, S. Bertolucci, M. Bragadireanu, M. Cargnelli, M. Catitti, C. Curceanu (Petrascu) et al., *New experimental limit on the Pauli exclusion principle violation by electrons*, *Physics Letters B* **641** (2006) 18.

[17] F. Napolitano, S. Bartalucci, S. Bertolucci, M. Bazzi, M. Bragadireanu, C. Capoccia et al., *Testing the Pauli Exclusion Principle with the VIP-2 Experiment*, *Symmetry* **14** (2022) 893.

[18] S. Manti, M. Bazzi, N. Bortolotti, C. Capoccia, M. Cargnelli, A. Clozza et al., *Testing the Pauli Exclusion Principle across the Periodic Table with the VIP-3 Experiment*, *Entropy* **26** (2024) .

[19] P. Vincent, H. Larochelle, I. Lajoie, Y. Bengio and P.-A. Manzagol, *Stacked Denoising Autoencoders: Learning Useful Representations in a Deep Network with a Local Denoising Criterion*, Journal of Machine Learning Research **11** (2010) 3371.

[20] M. Agostini, E. Bellotti, R. Brugnera, C.M. Cattadori, A. D'Andragora, A. di Vacri et al., *Characterization of a broad energy germanium detector and application to neutrinoless double beta decay search in 76Ge*, *Journal of Instrumentation* **6** (2011) P04005.

[21] K.-H. Ackermann, M. Agostini, M. Allardt, M. Altmann, E. Andreotti, A.M. Bakalyarov et al., *The Gerda experiment for the search of 0νββ decay in 76Ge*, *The European Physical Journal C* **73** (2013) 2330.

[22] M. Agostini, M. Allardt, E. Andreotti, A.M. Bakalyarov, M. Balata, I. Barabanov et al., *Pulse shape discrimination for Gerda Phase I data*, *The European Physical Journal C* **73** (2013) 2583.

[23] V.T. Jordanov and G.F. Knoll, *Digital synthesis of pulse shapes in real time for high resolution radiation spectroscopy*, *Nuclear Instruments and Methods in Physics Research Section A: Accelerators, Spectrometers, Detectors and Associated Equipment* **345** (1994) 337.